

NMR studies of the helium distribution in uranium tritide

Robert C. Bowman, Jr. and Albert Attalla

Mound Laboratory,* Monsanto Research Corporation, Miamisburg, Ohio 45342

(Received 20 April 1977)

The distribution of helium (^3He) created in uranium tritide (UT_3) by triton decay has been investigated by pulse NMR techniques. The line shapes and relaxation times for ^3He nuclei have been measured during a 3-year period. NMR samples were prepared from five UT_3 synthesis batches. Because UT_3 is a highly paramagnetic material which ferromagnetically orders below approximately 180 K, inhomogeneous magnetic field effects contributed to the NMR parameters. Detailed analyses of the frequency, temperature, and age dependences of these NMR parameters indicate most ^3He atoms are retained in microscopic gas bubbles with dimensions $< 500 \text{ \AA}$. No evidence was obtained to suggest significant concentrations of interstitial ^3He atoms in the UT_3 lattice. A simple model based upon the nucleation, growth, and subsequent rupture at critical dimensions of helium bubbles is presented. This model qualitatively describes the ^3He relaxation times and the observed ^3He retention in UT_3 powders.

I. INTRODUCTION

The transmutation of tritium into helium (^3He) provides an intense source of inert gas atoms in a host-metal tritide. Several previous studies¹⁻⁷ have indicated that many metal tritides can retain large quantities of helium prior to releasing helium to the gas phase. The physical state of the helium in these tritides is a very interesting and unresolved question. Namely, the atoms can be either individually dispersed in the host lattice (i.e., located in interstitial sites, vacancies, impurity-vacancy pairs, etc.) or trapped in clusters and gas bubbles. Although the presence of helium alters many physical properties of the host materials, most previous studies have not been able to provide a detailed microscopic understanding of the helium distribution in metal tritides. Helium gas bubbles have been observed in some studies,^{6,7} but evidence for the occupancy of octahedral interstitial sites in metal tritides with fluorite crystal structures have been recently reported.⁸

This paper reports a nuclear-magnetic-resonance (NMR) study of the distribution of ^3He in uranium tritide (UT_3). Since UT_3 is a good material for the storage and purification of tritium, it is expected to have many applications during the development of controlled thermonuclear reactors. Consequently, the helium retention of UT_3 has practical implications as well as providing another helium-metal tritide system to characterize. UT_3 retains nearly all the helium formed during the first several hundred days following synthesis before releasing significant quantities of helium gas. This behavior will be explained by a model based upon the formation and subsequent rupture of helium gas bubbles. Evidence for helium gas bubbles is provided by analyses of the ^3He relaxation times.

In principle, the NMR relaxation times are directly related to the physical state of the resonant-spin species. There are two limiting cases in which NMR can firmly establish the local environment. When the nuclei are situated in rigid lattice positions, the relaxation times obey the relations

$$T_{2d} \approx T_2^* \approx T_2 \ll T_1, \quad (1)$$

where T_{2d} is the dipolar spin-spin relaxation time which can be calculated using the Van Vleck⁹ formalism if the lattice sites are known, T_2^* is the linewidth relaxation time formally related to the experimental line shape, T_2 is the homogeneous spin-spin relaxation time, and T_1 is the spin-lattice relaxation time. The molecular motion in macroscopic quantities of bulk gas averages the dipolar interactions to zero and yields

$$T_{2d} \ll T_2^* < T_2 \approx T_1. \quad (2)$$

The differences in the nuclear-relaxation times for rigid and mobile species are dramatic with T_2^* and T_2 increasing by two to four orders of magnitude. However, there are also two possibilities for the relaxation times to have the intermediate behavior

$$T_{2d} < T_2^* < T_2 < T_1. \quad (3)$$

Relaxation times for nuclei diffusing rapidly in the solid lattice obey either Eq. (2) or Eq. (3) depending on the mobilities, strength of dipolar interactions, and presence of inhomogeneous magnetic fields. On the other hand if the dimensions of gas bubbles are sufficiently small (i.e., dimensions $\lesssim 1000 \text{ \AA}$), collisions with wall surfaces will dominate¹⁰ the relaxation rates and will reduce T_2^* and T_2 relative to T_1 , and Eq. (3) will correspond to the relaxation times. Analyses of the frequency and temperature dependence of the relaxation times can distinguish between wall interactions in microscopic gas bub-

bles and bulk diffusion in solid lattice. For ^3He spins the same general considerations are valid with the addition of spin exchange effects¹¹ occurring at low temperatures and high densities. Unfortunately, complications arising from large inhomogeneities can occur¹² for paramagnetic materials and analyses become less straightforward. Nevertheless, the present NMR studies of UT_3 illustrate that ^3He relaxation times provide valuable insights on the distribution of helium atoms in metal tritides.

II. EXPERIMENTAL PROCEDURES

Five preparations of UT_3 have been examined by NMR techniques. The tritides were synthesized by heating chips or rods of uranium metal to ~ 675 K and exposing them for several hours to pure tritium gas. Fine powders with surface areas of $0.40\text{--}0.85$ m^2/g were produced. The assumption¹³ of uniform particle sizes results in calculated average diameters of $0.6\text{--}1.3$ μm . X-ray diffraction measurements indicated the crystal structure of UT_3 is the same as β -phase UH_3 (i.e., space group $Pm\bar{3}n$) with an initial lattice constant $a_0 = 6.625 \pm 0.005$ \AA . These findings are in excellent agreement with the results reported by Johnson *et al.*¹⁴ The UT_3 powders were stored in metal containers under argon atmospheres prior to loading into 9-mm-o.d. pyrex sample tubes which were evacuated and sealed.

Pulse NMR techniques have been used to determine the ^3He nuclear relaxation times. Because the ^3He free-induction-decay (FID) signals are very short and the electronic recovery time and probe ringing often obscure the NMR signals for $50\text{--}100$ μsec , T_2^* was determined by analyzing the line shape of spin echoes produced by a $\frac{1}{2}\pi\text{--}\pi$ pulse sequence. The spin-spin relaxation time T_2' was obtained from the dependence of the spin echo maxima on the spacing τ between the $\frac{1}{2}\pi$ and π pulses. However, the spin echo technique often does not completely remove¹² the inhomogeneous contributions from T_2' . Consequently, the homogeneous spin-spin relaxation time T_{2m} was determined using the Carr-Purcell-Meiboom-Gill (CPMG) pulse sequence.¹⁵ Zamir and Cotts¹² have shown the CPMG sequence minimizes the effects of magnetic field gradients on T_{2m} although a complete removal of the inhomogeneous effects is not achieved because of the finite spacing between the π pulses. The gradient effects are the largest for rapid diffusion in high-susceptibility materials such as UH_3 or UT_3 . The ^3He T_1 relaxation times were measured using the $\pi\text{--}\tau\text{--}\frac{1}{2}\pi\text{--}100$ $\mu\text{sec}\text{--}\pi$ pulse sequence.

In addition to nuclear relaxation times, ^3He concentrations in UT_3 were determined by NMR spin counting techniques. The amplitudes of the ^3He

spin echo maxima extrapolated to zero spacing between the pulses were compared with the initial heights of the FIDs of standard samples. The spin standards were protons in $\text{H}_2\text{O}/\text{D}_2\text{O}$ solutions containing small quantities of MnCl_2 to shorten T_1 . Relative sensitivity corrections have been made between the ^3He and proton spin counts. The precision of the spin counts is approximately $\pm 10\%$. Independent determinations of the ^3He concentration are provided by volumetric-mass spectrometric analyses of the gases released during thermal decomposition to ~ 1300 K.

The NMR measurements were performed with a Bruker variable frequency *BKR-323s* pulse spectrometer. Because the ^3He resonance signals were generally weak and also required large receiver bandwidths due to short decay times, extensive signal averaging was necessary for quantitative evaluation of the ^3He relaxation times. The signals were digitized by a Biomation 8100 transient recorder and stored in the memory of a Nicolet 1074 signal averager for signal-to-noise ratio enhancement and baseline subtraction. The majority of the relaxation times were obtained at 20.00 MHz and room temperature (i.e., between 292 and 295 K) except when frequency and temperature dependences were investigated. The ^3He relaxation times are normally reproducible within $\sim 10\%$. Since the T_1 and the CPMG echoes decay nonexponentially, these relaxation times are defined as the time at which the signals have decayed to $1/e$ of their initial values.

III. CHARACTERISTICS OF ^3He RELAXATION TIMES

A. ^3He NMR line shapes

Since the UT_3 samples are isomorphic with β -phase UH_3 , UT_3 is expected to be ferromagnetic below ~ 180 K the same as $\beta\text{-UH}_3$ and $\beta\text{-UD}_3$. Consequently, UT_3 is paramagnetic above the Curie temperature θ with a large temperature-dependent magnetic susceptibility. The NMR parameters for nonmagnetic nuclei such as the hydrogen isotopes or ^3He strongly reflect the paramagnetic character of UH_3 or UT_3 . For examples, the proton and deuteron NMR line shapes in UH_3 and UD_3 have been measured by Grunzweig-Genossar *et al.*,¹⁶ and the corresponding second moments M_2 were found to obey the relation

$$M_2 = M_{2D} + M_{2Q} + M_{2P}h^2, \quad (5)$$

where

$$h = H_0/(T - \theta).$$

Here, M_{2D} is the internuclear dipolar contribution, M_{2Q} is the quadrupolar term which vanishes when the nuclear-spin quantum number is $\frac{1}{2}$ (i.e., for

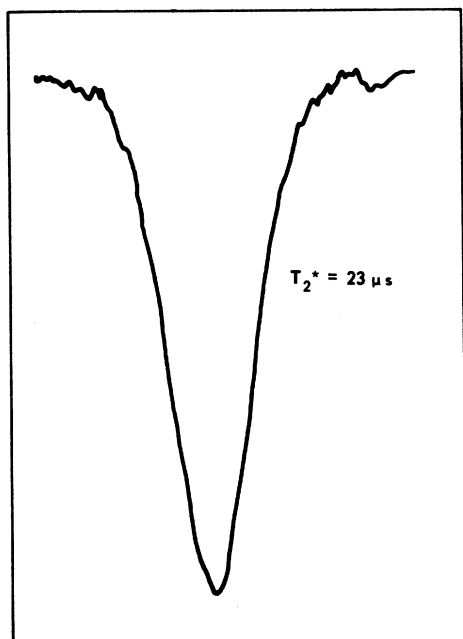


FIG. 1. Experimental ^3He spin-echo resonance signal at 20.0 MHz for UT_3 aged 2 years (sample A).

H, T, and ^3He nuclei), M_{2P} is a magnetic field-dependent term which arises from the electron-nuclear interactions with uranium $5f$ electrons and the magnetic field gradients produced¹⁷ by the powder structure of the samples, H_0 is the magnetic field strength, T is the absolute temperature, and $\theta \approx 183$ K. If the ^3He atoms are not located on UT_3 lattice sites, only the demagnetization field from

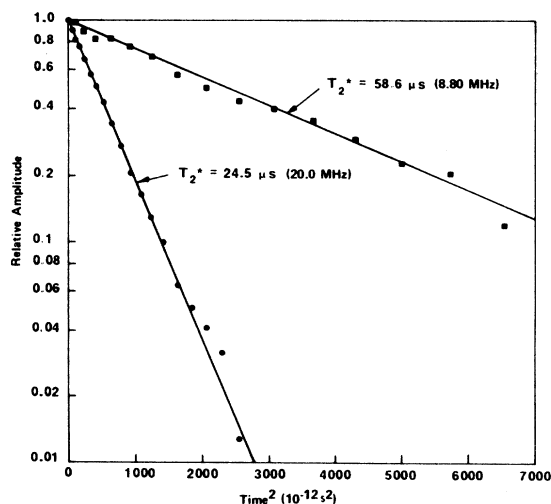


FIG. 2. Gaussian plots of the ^3He line shapes at 8.8 and 20.0 MHz for 2-year-old sample A.

the powder particles contribute to M_{2P} . Grunzweig-Genossar *et al.*¹⁶ analyzed the demagnetization effects for $\beta\text{-UH}_3$ and obtained

$$M_{2V} = 2 \times 10^{-3} \text{ h}^2 \text{ G}^2, \quad (6)$$

where M_{2V} is the contribution of powder structure to the second moment. When the electron-nuclear interactions are included, Grunzweig-Genossar *et al.* calculated

$$M_{2P} = 4.5 \times 10^{-3} \text{ h}^2 \text{ G}^2 \quad (7)$$

for both UH_3 and UD_3 . Similar values of M_{2V} and M_{2P} are expected for UT_3 since the susceptibilities and effective-particle sizes (i.e., $\sim 1 \mu\text{m}$) are nearly the same as reported¹⁶ for UH_3 and UD_3 .

A typical ^3He spin-echo signal at 20 MHz is presented in Fig. 1. Because the T_2^* is only $23 \mu\text{sec}$, the FID is obscured by probe recovery times and the line shapes must be measured from the echoes. Normalized plots of the ^3He line shapes obtained from echoes at 8.8 and 20 MHz are given in Fig. 2. Two important observations can be made from these plots. First, the ^3He line shapes are Gaussian. Thus, the ^3He second moment M_2' can be obtained using the expression

$$M_2' \doteq 2/(\gamma T_2^*)^2, \quad (8)$$

where γ is the ^3He gyromagnetic ratio. Second, T_2^* (i.e., the ^3He linewidth) is very dependent upon the resonance frequency ν (i.e., magnetic field strength through $\nu = \gamma H_0$). The magnetic field dependence of the ^3He second moments measured for 2.3-year-old UT_3 (sample A) is presented in Fig. 3. The measurements were performed at room

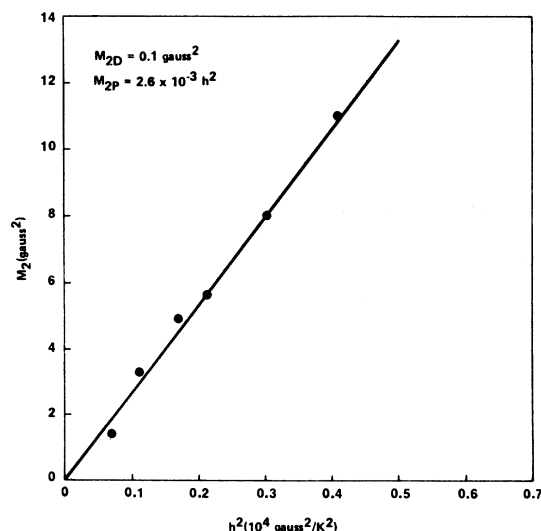


FIG. 3. Magnetic field dependence of ^3He second moments in 2.3-year-old UT_3 (sample A) at room temperature.

temperature; M'_2 was calculated using Eq. (8) and the T_2^* obtained from Gaussian plots of the echo line shapes. The extrapolated zero field quantity (i.e., M_{2D}) is $\sim 0.1 \text{ G}^2$.

When the locations of the magnetic nuclei are known, the rigid-lattice dipolar term M_{2D} can be predicted using the Van Vleck⁹ formalism. The general theoretical expression for the ^3He M_{2D} term is

$$M_{2D} = \left[\frac{3}{5} \gamma^2 \hbar^2 f_I I(I+1) \right] \sum_i r_i^{-6} + \left[\frac{4}{15} \gamma^2 \hbar^2 f_S S(S+1) \right] \sum_j r_j^{-6}, \quad (9)$$

where I is the ^3He -spin quantum number, S is the tritium-spin quantum number, γ_I and γ_S are the respective gyromagnetic ratios, f_I and f_S are the fractional sites occupancies for ^3He and T spins, \hbar is Planck's constant divided by 2π , $\sum_i r_i^{-6}$ is the lattice sum for He-He interactions, and $\sum_j r_j^{-6}$ is the lattice sum for ^3He -T interactions. In addition, ^3He and T spins are each assumed to occupy only one type of lattice site. The dipolar interactions of ^3He with H , D , and ^{235}U nuclei are neglected in Eq. (9) since the concentrations of these latter species are negligible. If the ^3He spins are further assumed to be located on tritium lattice sites (i.e., where ^3He nuclei are produced during triton decay), the lattice sums $\sum_i r_i^{-6}$ and $\sum_j r_j^{-6}$ are equal to the H-H dipolar lattice sum evaluated by Grunzweig-Genossar *et al.*¹⁶ The calculated M_{2D} with the ^3He atoms in tritium sites for the 2.3-year-old sample *A* in Fig. 3 is 12.0 G^2 . Since the experimental zero field value of $\sim 0.1 \text{ G}^2$ is two orders of magnitude smaller than the theoretical dipolar M_{2D} value, the ^3He resonance linewidth in UT_3 is not dipolar broadened. If nuclear-exchange effects can be neglected (which is reasonable considering other data to be presented later in this paper), the only ^3He distributions in 2.3-year-old UT_3 consistent with an experimental M_{2D} of $\sim 0.1 \text{ G}^2$ are as follows: (i) ^3He atoms occupy tritide lattice sites, but the ^3He diffusion rate is very high and greatly reduces the dipolar interactions from the rigid lattice value of 12 G^2 . (ii) ^3He atoms are trapped in clusters or microscopic gas bubbles, which have formed in the solid lattice, and exhibit the nuclear-relaxation times characteristics of Eq. (3).

Although the dipolar M_{2D} have not been explicitly calculated for other possible rigid ^3He distributions in UT_3 (e.g., ^3He in various interstitial sites) due to the lack of evaluated lattice sums, the theoretical M_{2D} should not change significantly (i.e., within a factor of ~ 2) from the value assuming ^3He on tritium lattice sites. Hence, a two-orders-of-magnitude difference between dipolar and experi-

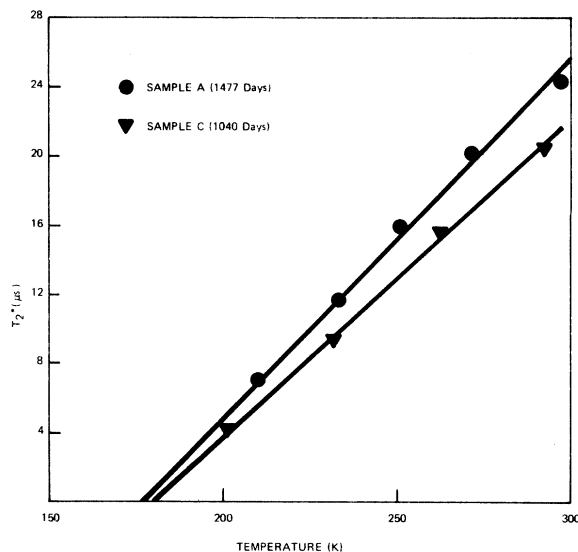


FIG. 4. Temperature dependence of T_2^* for ^3He resonance at 20 MHz in UT_3 .

mental M_{2D} would still occur.

The field-dependent term of the experimental M_2 provides evidence for ^3He gas bubbles. Namely, the M_{2P} value of $2.6 \times 10^{-3} \text{ h}^2$ for UT_3 is very close to the M_{2V} of Eq. (6) where only the demagnetization fields from powder grains are included. If ^3He atoms are located on tritium lattice sites, the electron-nuclear interactions should also contribute and yield a total M_{2P} approximately equal to the larger value of Eq. (7). Hence, the experimental M_{2P} for ^3He suggests the ^3He atoms are not located in the UT_3 lattice. Since the particle size distribution and susceptibility of UT_3 is not expected to be equal to the UH_3 and UD_3 samples of Grunzweig-Genossar *et al.*, exact agreement between ^3He M_{2P} and M_{2V} is not expected. However, these values are consistent with helium gas bubbles in the lattice.

The temperature dependence of the ^3He linewidth T_2^* measured at 20 MHz for two UT_3 samples is presented in Fig. 4. In addition, spin-echo measurements indicate the ^3He echo has essentially disappeared below 175 K. This behavior for the echo magnitude and T_2^* occurs because UT_3 becomes ferromagnetic near $\sim 180 \text{ K}$. Hence, the resulting intense internal magnetic fields produce major shifts in the ^3He resonance frequency as well as extensive line broadening from the field gradients. Because of tritium decay, the UT_3 will be substoichiometric (possibly, with variable composition for individual particles) which can change θ or lead to a distribution of θ values near $\sim 180 \text{ K}$. Hence, the observation of a small amount of ^3He magnetization below $\sim 180 \text{ K}$ is still consistent with

complete ferromagnetic ordering in UT_3 . A detailed investigation of the NMR was not performed below ~ 200 K since the evaluation of magnetic ordering in UT_3 was not an objective of the present study. However, since the ^3He linewidth parameter T_2^* exhibits a $(T - \theta)$ dependence above the Curie temperature as shown in Fig. 4, the inhomogeneous M_{2p} term clearly dominates the ^3He line shape in the highly paramagnetic UT_3 .

B. Spin echoes

The decays of ^3He spin-echo maxima for four UT_3 samples of different ages (i.e., ^3He concentrations) are presented in Fig. 5. The relaxation times T_2' obtained from the echo decays increase with age which is opposite the behavior predicted for dipolar interactions between immobile ^3He spins. When the dipolar interactions between like spins are much smaller than between unlike spins for a two-spin system (i.e., ^3He and T in UT_3), the spin-echo decay is directly related¹⁸ to the like spin component of the dipolar second moment. The dipolar interactions with the nonresonant spins behave as an inhomogeneous magnetic field. Consequently, only the first term in Eq. (9) would contribute to the echo decay for ^3He atoms in the UT_3 lattice. Since f_I increases as the ^3He concentration increases, the ^3He - ^3He dipolar second moment would become larger and the corresponding T_2' decrease with age if ^3He occupies lattice sites. Using the previous assumptions for immobile helium on tritium sites and a constant lattice constant of 6.625 \AA , T_2' is calculated to decrease from 0.17 to 0.05 msec as the

sample age increases from 83 to 899 days. However, the experimental T_2' from Fig. 5 are found to increase more than an order of magnitude between these ages. Consequently, the T_2' values confirm the previous linewidth studies that ^3He atoms are not located on rigid-lattice sites in UT_3 . If significant quantities (i.e., $\sim 10^{20}$ atoms/g UT_3) of ^3He were rigidly located on UT_3 lattice sites, the echo decays in Fig. 4 would show an additional initial decay with $T_2 \sim 0.1$ msec. The absence of these rapid decays strongly suggests the concentration of immobile ^3He in UT_3 is also below this limit.

It is conceivable that not all ^3He spins are contributing to the NMR signals. Those ^3He atoms on UT_3 lattice sites may not be detected because of very short T_2' or other experimental difficulties. However, the extrapolated spin echo amplitudes are proportional to the concentrations of spins detected by NMR. The ^3He spin counts obtained with the previously described procedures yielded¹⁹ ^3He concentrations which were $\sim 85\%$ – 90% of the ^3He gas evolved during quantitative thermal decompositions. Since the values for these two methods are within the expected errors of the spin counting techniques, this agreement indicates all (within the sensitivity limits for NMR) the ^3He atoms in UT_3 are being characterized by the NMR parameters. Hence, in contrast to the behavior recently reported⁸ for TiT_x , the ^3He atoms formed in UT_3 are not retained in "rigid"-lattice sites. There is no evidence for immobile ^3He atoms in UT_3 in times as short as ~ 100 days; only ^3He atoms with sufficient mobility to greatly reduce the static dipolar interactions have been observed during NMR studies for the UT_3 samples. The Gaussian line shapes and very short T_2^* values for ^3He are caused by the inhomogeneous magnetic fields arising from the paramagnetic UT_3 particles and not by dipolar interactions among "rigid" ^3He atoms on UT_3 lattice sites.

C. Relaxation times T_1 and T_{2m}

The ^3He relaxation times T_1 and T_{2m} provide additional insight into the distribution of helium in UT_3 . Since the ^3He -spin quantum number is $\frac{1}{2}$, quadrupolar contributions to the nuclear relaxation processes are absent. Hence, interpretation of the ^3He relaxation-time data is not complicated by various esoteric mechanisms which often influence quadrupolar relaxations. Only the conventional nuclear dipole-dipole, various paramagnetic, and spin exchange effects are expected^{20,21} to be possible contributors to ^3He relaxation in UT_3 . Evidence for this behavior is provided by the preliminary pulse NMR measurements of tritium resonance at 20 MHz in UT_3 . The approximate values for the tritium parameters obtained at room temperature are (a) $T_1 \approx 4$ msec, in excellent agree-

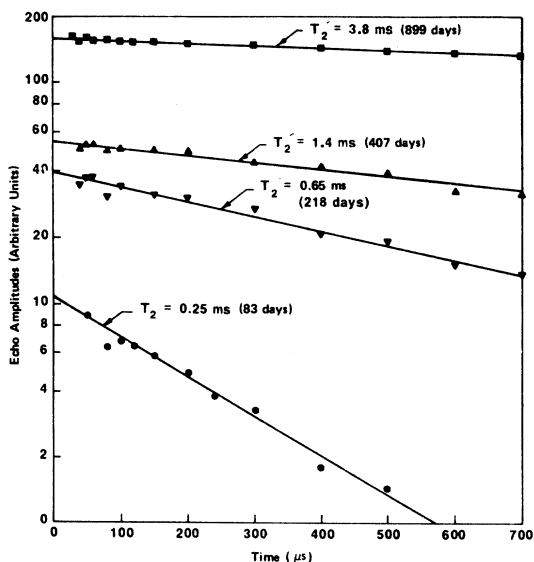


FIG. 5. Decays of ^3He spin-echo maxima at 20.0 MHz and room temperature.

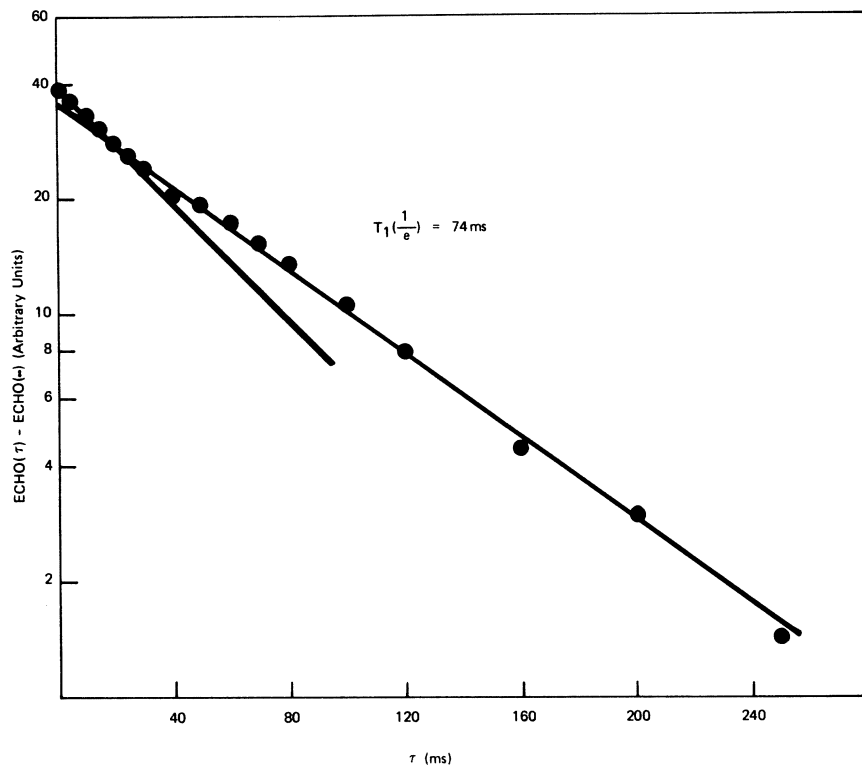


FIG. 6. Typical example of recovery of the ^3He magnetization in UT_3 (sample E aged for 837 days at room temperature) at 20 MHz.

ment with the T_1 data reported by Cinader *et al.*²⁰ for protons in UT_3 ; (b) $T_2^* < 10 \mu\text{sec}$, which is consistent with results of Grunzweig-Genossar *et al.*¹⁶ for "rigid-lattice" protons in UH_3 . Weaver²² has obtained tritium second moments of 30 and 31 G^2 at 16.0 MHz from cw measurements on material from two of the UT_3 samples. These values and Eq. (8) yield tritium T_2^* of 9.0 and 8.9 μsec in agreement with the more qualitative pulse NMR results; and (c) tritium Knight shift $K_T \approx 2 \times 10^{-3}$ in good agreement with the literature value¹⁶ for protons in UH_3 and the cw measurements by Weaver²² for UT_3 .

Since the NMR parameters for tritium in UT_3 exhibit the same characteristics as the proton parameters in UH_3 , similar nuclear relaxation processes occur for both systems. Consequently, the ^3He relaxation in UT_3 should be dominated by the contributions previously proposed^{21,22} for UH_3 (possibly modified for exchange effects) unless the helium atoms are trapped in gas bubbles which can significantly reduce the UT_3 lattice effects.

Representative examples of ^3He magnetization recoveries during the T_1 measurements and the decay of the even echo maxima formed by the CPMG sequence are given in Figs. 6 and 7, respectively. Although these data were obtained on 837-day-old sample E , the general form of the nonexponential recoveries (i.e., an initial rapid decay followed by a

more slowly decaying tail) is typical for the ^3He relaxation-time measurements regardless of sample or age. The degree of nonexponential behavior varies widely and is often far greater than the examples in Figs. 6 and 7; however, no correlation with the macroscopic sample properties or age has been deduced. A consistent method of evaluating the relaxation times is required to compare the recovery data obtained from several samples over the ~ 3 -year period of these studies. It was decided to define the relaxation times T_1 and T_{2m} as the time the magnetization and echo maxima have reached $1/e$ of the value of the initial data point. Although this procedure is an oversimplification which reduces complex recoveries to single parameters, it does provide a convenient analytic method for determining the gross features of helium distribution from ^3He nuclear-relaxation behavior. In fact, nonexponential recoveries without unique solutions for the corresponding relaxation times can be readily rationalized for several plausible helium distributions and will be discussed later in this paper. However, for the present analyses the ^3He relaxation times are represented by the exponential values defined above.

An important feature of the CPMG measurements is the decrease of T_{2m} as the spacing (2τ) between the π pulses increases. This behavior is illustrated in Fig. 8 for 3.3-year-old UT_3 sample where T_{2m}^{-1}

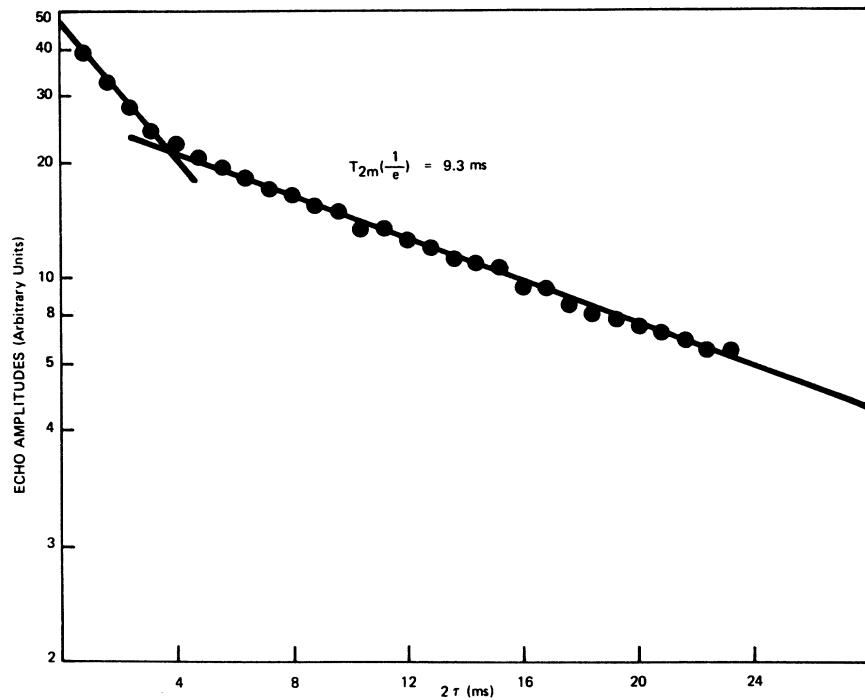


FIG. 7. Typical echo maxima decay for CPMG pulse sequence (2τ spacing of $400 \mu\text{sec}$) for ^3He in UT_3 at 20 MHz. Measurements on 837-day-old sample E.

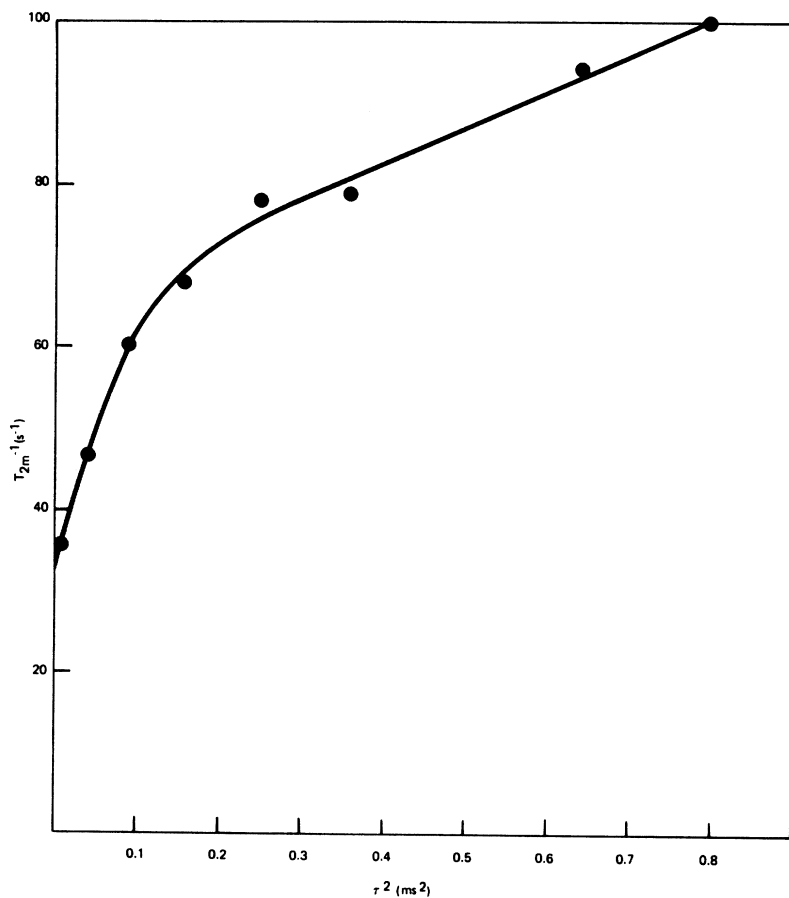


FIG. 8. Effect of spacing (2τ) between π pulses in CPMG sequence on T_{2m}^{-1} for ^3He at 20 MHz. Measurements on sample A aged for 3.3 years.

is plotted with τ^2 . Zamir and Cotts¹² have shown that rapid diffusion in a strong magnetic gradient is responsible for the T_{2m} decrease and they obtained

$$T_{2m}^{-1} = T_2^{-1} + \frac{1}{3}\gamma^2 G^2 D \tau^2, \quad (10)$$

where the gradient G is given by

$$G = 3\chi H_0/L. \quad (11)$$

Here, the "true" spin-spin relaxation time T_2 is free of inhomogeneous contributions, D is the diffusion constant, the bulk susceptibility χ is $\sim(T - \theta)^{-1}$ for UT_3 , and the characteristic length L is proportional to both the diffusion path length and the particle size of the powder. The nonlinear plot in Fig. 8 is believed to arise mainly from a distribution in G values for the nonuniform L dimensions of the irregular UT_3 sample. Although a quantitative analysis of T_{2m} dependence on τ^2 is not possible due to incomplete knowledge of the effective L distribution for the UT_3 sample, the extrapolated value $T_2 = 31$ msec is obtained in the limit of zero spacing between the π pulses. Since $T_1 = 92$ msec for ${}^3\text{He}$ in this sample at 3.3 year, the homogeneous T_2 does not equal T_1 which is predicted^{12,23,24} for extremely rapid diffusion in either solids or bulk gases. Hence, either the ${}^3\text{He}$ diffusion rate is insufficient to yield $T_1 \approx T_2$ or an additional mechanism reduces T_2 relative to T_1 for rapidly diffusing ${}^3\text{He}$ atoms. Evidence favoring the second possibility will be presented shortly.

The frequency dependences of the ${}^3\text{He}$ relaxation times T_2^* , T_{2m} , and T_1 for 2.5-year-old UT_3 are summarized in Table I. These values were obtained at room temperature and the spacing between the CPMG π pulses was 400 μsec . At each frequency the relaxation times obey the general relations of Eq. (3). The decrease of T_2^* with frequency, which agrees with results presented in Figs. 2 and 3, is due to the increase of the total second moment with magnetic field strength as described in Sec. IIIA. The frequency dependences of the ${}^3\text{He}$ relaxation

times in Table I strongly indicate spin-exchange interactions are not the dominant relaxation mechanism for ${}^3\text{He}$ nuclei in UT_3 . Namely, both T_{2m} and T_1 must increase with frequency if the exchange interactions are primary contributors to nuclear relaxation.^{11,25,26} Since T_1 decreases and T_{2m} initially decreases followed by an approximately constant value as the frequency increases, exchange cannot be a significant factor for ${}^3\text{He}$ relaxation. Hence, the possibility of immobile ${}^3\text{He}$ atoms with strong exchange interactions can be excluded as a plausible model for helium retention in UT_3 , which justifies the neglect of exchange contributions during the earlier analyses of T_2^* and T_2' .

The temperature dependences of the ${}^3\text{He}$ relaxation times T_{2m} and T_1 have been measured at 20 MHz for a 2.85-year-old UT_3 sample and are shown in Fig. 9. Both ${}^3\text{He}$ relaxation times are observed to decrease as the temperature approaches θ and no evidence for a minimum value of T_1 was detected between 200 and 300 K. The T_{2m}/T_1 ratio remains nearly constant throughout this temperature range. Similar temperature dependences for ${}^3\text{He}$ relaxation was observed in two other UT_3 samples at different ages. Hence, the results in Fig. 9 are regarded as representative for ${}^3\text{He}$ relaxation behavior in UT_3 .

The observed temperature and frequency dependences for T_{2m} and T_1 in Fig. 9 and Table I will be compared for two most plausible helium distributions in UT_3 : (a) mobile ${}^3\text{He}$ atoms on lattice sites; and (b) microscopic helium-gas bubbles. The analyses most directly correspond to UT_3 samples that have been at room temperature for ~ 3 years. However, the general conclusions should be valid for any age or ${}^3\text{He}$ concentration in UT_3 , providing the ${}^3\text{He}$ relaxation times obey Eq. (3).

The relationship between nuclear-relaxation times and atomic motion in metal hydrides is well established and numerous examples have been reported.²⁴ In the case of hydrogen diffusion in UH_3 , the exponential correlation time model²⁴ has been used to analyze^{20,21} both T_1 and T_2 data and yielded a fairly complete understanding of hydrogen transport. The measured proton T_1 has three contributions:

$$1/T_1 = 1/T_{1f} + 1/T_{1K} + 1/T_{1D}. \quad (12)$$

Here, the Ruderman-Kittel-Kasuya-Yosida (RKKY) interaction which arises from an indirect interaction between localized paramagnetic $5f$ electrons through the conduction electrons yields $T_{1f}^{-1} \sim T/(T - \theta)$; the contact interaction with the conduction electrons produces the Korringa term $T_{1K}^{-1} = C_K T$; and T_{1D} is the diffusion sensitive nuclear dipolar term. The mobility of protons in UH_3 is relatively

TABLE I. Frequency dependence of ${}^3\text{He}$ relaxation times in 2.5-year-old UT_3 as measured at room temperature.

ν (MHz)	T_2^* ^a (μsec)	T_{2m} ^b (m sec)	T_1 (m sec)
8.8	55.8	25	90
20.0	26.2	16.5	85
30.0	16.2	19	70
45.7	15.0	18	66.5

^aSpin echo with $\tau = 150 \mu\text{sec}$.

^bCPMG with $2\tau = 400 \mu\text{sec}$.

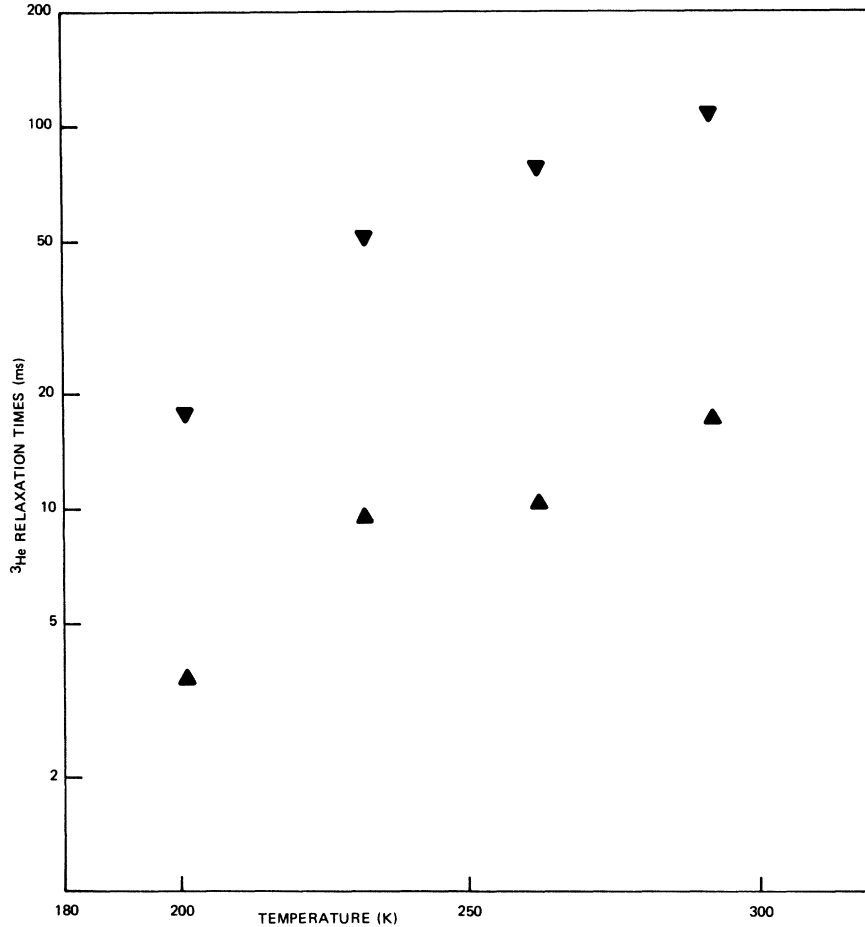


FIG. 9. Temperature dependence of ${}^3\text{He}$ relaxation times T_{2m} (\blacktriangle) and T_1 (\blacktriangledown) in 1040-day-old UT_3 (sample C). Measurements performed at 20 MHz where CPMG pulse spacing was 400 μsec between π pulses.

low since measurable proton spin echoes are first observed²¹ above ~ 500 K and the diffusion induced minimum in T_1 occurs²⁰ ~ 610 K. A relatively high-proton activation energy $E_a = 0.8$ eV for a metal hydride²⁴ was deduced from these studies. Hence, the T atoms in UT_3 are predicted to be essentially immobile at room temperature where the tritium relaxation times obey Eq. (1).

The exponential correlation model²⁴ for ${}^3\text{He}$ diffusion in UT_3 yield the general expressions

$$T_{1D}^{-1} = \frac{2}{5}C_S \left[\frac{1}{3}F(\omega_I - \omega_S) + F(\omega_I) + 2F(\omega_I + \omega_S) \right] \sum_j r_j^6, \quad (13)$$

$$T_{2D}^{-1} = \frac{2}{5}C_S \left[\frac{2}{3}F(0) + \frac{1}{6}F(\omega_I - \omega_S) + \frac{1}{2}F(\omega_I) + F(\omega_S) + F(\omega_I + \omega_S) \right] \sum_j r_j^6, \quad (14)$$

where

$$F(\omega) = \tau_c / (1 + \omega^2 \tau_c^2), \quad (15)$$

$C_S = \gamma_I^2 \gamma_S^2 \hbar^2 S(S+1)$, $\omega_I = \gamma_I H_0$, $\omega_S = \gamma_S H_0$, subscripts I and S refer to helium and tritium nuclei, respectively, τ_c is the diffusion correlation time, and the summation refers to tritium sites with the origin at a helium site. The ${}^3\text{He}$ - ${}^3\text{He}$ dipolar contribution has been neglected since it is much smaller than the ${}^3\text{He}$ -T term. For example, when the ${}^3\text{He}$ atoms occupy tritium lattice sites, the ${}^3\text{He}$ - ${}^3\text{He}$ term is ~ 10 times smaller than the ${}^3\text{He}$ -T term for 3-year-old UT_3 . The assumption of Arrhenius temperature dependence for diffusion yields

$$\tau_c = \tau_0 \exp(E_a/kT). \quad (16)$$

If diffusion is a major ${}^3\text{He}$ relaxation mechanism, the following characteristics are derived from Eqs. (13)–(16): (i) A minimum in T_1 , $T_{1\text{min}}$, occurs when $\omega \tau_c \approx 1$ and $T_{1\text{min}} \propto \omega$. (ii) At low temperatures ($\omega^2 \tau_c^2 \gg 1$) $\ln T_1 \propto T^{-1}$, $T_1 \propto \omega^2 \tau_c$, $T_2 \propto M_2 / \tau_c$, and $T_2 < T_1$. (iii) At high temperatures $\ln T_1 \propto T$, T_1 is independent of ω , and $T_2 \approx T_1$. When the ${}^3\text{He}$ relaxation times in Fig. 9 and Table I are evaluated with respect to diffusion contributors, several dif-

difficulties are encountered. The absence of a $T_{1\min}$ down to ~ 200 K, increase of T_1 with temperature, and long T_2 (i.e., T_2/T_1 ratio of ~ 0.2 between 200 and 300 K) would imply very rapid diffusion, $\omega^2\tau_c^2 \ll 1$; however, T_1 at 300 K should be independent of frequency and not decrease with ω as shown in Table I. If the helium diffusion rate is insufficient to yield a $T_{1\min}$, T_2 would be much smaller than T_1 and the ratio T_2/T_1 increases as the temperature is raised. Figure 9 shows both of these statements to be incorrect. Furthermore, T_1 should decrease with temperature below $T_{1\min}$ and increase, not decrease, with ω if T_{1D} dominates ^3He spin-lattice relaxation. Since the assumption of diffusion relaxation leads to inconsistencies with the observed ^3He relaxation times in ~ 3 -year-old UT_3 , rapid helium diffusion between tritide lattice sites seems to be an unlikely explanation.

Since the observed ^3He relaxation times are incompatible with the other explanations for the physical state of ^3He in UT_3 , the final alternative to be considered is gaseous ^3He trapped in microscopic gas bubbles. This gas is chemically pure and the concentration of paramagnetic impurities such as oxygen is expected to be extremely small as the bubbles are formed by triton decay in the interior of the UT_3 particles. Any oxygen in the system should react at tritide or metal surfaces to form very stable UO_2 . Hence, ^3He relaxation times are determined only by the bulk properties of the gas and surface interactions with the bubble wall. A phenomenological expression for the spin-lattice relaxation is

$$T_1^{-1} = T_{1B}^{-1} + T_{1W}^{-1}, \quad (17)$$

where the form²⁷ of the bulk relaxation time T_{1B} changes with density and T_{1W} is the wall relaxation time. For sufficiently impure surfaces the spin-flip probability per wall collision α is large (i.e., ~ 1) and

$$T_1 = R^2/\pi^2 D \quad (18)$$

for a spherical bubble of radius R and a diffusion constant D . On the other hand, if $\alpha \ll 1$, the relaxation time is

$$T_{1W} = 4R/3\alpha[v], \quad (19)$$

where $[v]$ is the average thermal velocity. In this case T_{1W} will only be weakly dependent on the gas density through α . In the limit of rapid diffusion within restricted dimensions (i.e., bubbles with mean dimensions $\lesssim 1000$ Å), an approximate expression for the spin-spin relaxation has been derived¹⁰ in the form

$$T_2^{-1} = T_{2B}^{-1} + (2\lambda/d)T_{2W}^{-1}, \quad (20)$$

where d is the bubble diameter, the bulk gas re-

laxation time $T_{2B} \approx T_{1B}$, and T_{2W} is the spin-spin relaxation time at the surface layer of characteristic width λ . The nature of the relaxation mechanisms at surfaces is not fully understood. However, suppression of gas atom mobility during collisions with bubble walls provides opportunity for semistatic dipolar interactions between neighboring ^3He atoms near the wall as well as dipolar interactions with the paramagnetic wall. The longest values for T_{2W} , in the limit of rapid mobility near the surface and small α , should correspond to the T_{1W} in Eq. (19).

In order to compare the ^3He relaxation times T_1 and T_{2m} in Fig. 9 and Table I with predictions for microscopic ^3He bubbles, the properties of the bubbles in ~ 3 -year-old UT_3 must be estimated. The bubbles are assumed spherical with a mean radius R_m . Since bubbles have not been observed in aged UT_3 during scanning electron microscopy studies,²⁸ R_m must be $< (250-500)$ Å. These bubbles are further assumed to be in equilibrium with the surface tension Γ of the lattice which yields²⁹ very high pressures of $\sim 10^3-10^4$ atm in the bubbles. Assuming a Γ of 1000 erg/cm², Evans³⁰ has calculated a density ρ of 4.5×10^3 He atoms/cm³ for a bubble with a 25 -Å radius. Evans also found that ρ decreased slowly as the bubble radius is increased. Although Evans performed his calculations for helium implanted metals, the conclusion of high, nearly constant density for the helium gas bubbles should also be valid for the metallic UT_3 system.

The bulk relaxation time T_{1B} for ^3He nuclei in high-density fluids is given by the expression^{27,31}

$$T_{1B} = D/C_B\rho, \quad (21)$$

where measurements³¹ in liquid ^3He yielded $C_B = 2.6 \times 10^{-6}$ cm⁵/g sec² and C_B is independent of pressure and temperature. The diffusion constant in gaseous ^3He approximately obeys

$$\rho D = D_0. \quad (22)$$

Karra and Kemmerer³² obtained $D_0 = 0.7$ amagat cm²/sec (1 amagat = 2.5×10^{19} atom/cm³) for ^3He gas at room temperature with 4% O_2 impurity. Assuming $\rho = 4.5 \times 10^{22}$ atoms/cm³ for ^3He bubbles in UT_3 , Eqs. (21) and (22) yield $T_{1B} \approx 660$ sec which is nearly three orders of magnitude larger than the room temperature T_1 in Table I. Hence, the bulk gas contribution to T_1 as well as to T_2 can be completely neglected for ^3He bubbles in UT_3 .

Since the ^3He bubble walls in UT_3 should be free of paramagnetic impurities, only the intrinsic paramagnetism of the UT_3 lattice contributes to T_{1W} , which obeys Eq. (19) for this relatively weak relaxation mechanism. Processes resulting in slowed

motion at the surface are the most effective in relaxing ^3He spins. Adsorption at temperatures below ~ 100 K and permeation of ^3He into the surface walls near and above room temperature are known³³⁻³⁵ to efficiently relax ^3He spins. However, neither mechanism is important for gas bubbles in UT_3 above 200 K since ^3He should be insoluble in the UT_3 lattice and adsorption does not occur at these temperatures. Hence, relaxation in UT_3 occurs only during the sticking time t_s of the collision with the bubble wall and the spin flip probability can be approximately expressed by the relation

$$\alpha = t_s/T_{1S} \quad (23)$$

where T_{1S} is the relaxation time at the surface and $t_s \ll T_{1S}$. Substitution of Eq. (23) into Eq. (19) yields

$$T_{1W} = (4R_m/3[v]t_s)T_{1S} \quad (24)$$

for ^3He bubbles of mean radii R_m . The sticking time per collision is approximately 10^{-13} sec since adsorption does not occur at the surface.³³ Although it is impossible to accurately specify T_{1S} for ^3He nuclei in UT_3 , T_{1S} can be assumed to be approximately equal to the T_1 for tritium, which is dominated by the RKKY electron interaction T_{1f} below 400 K. If the ^3He distribution in 3-year-old UT_3 consists of bubbles with uniform 25-Å radii, the room temperature T_{1W} is calculated as

$$T_{1W} = 92 \text{ msec} \quad (25)$$

at 20 MHz where $T_{1S} \approx 4$ msec from the tritium T_1 and the ^3He thermal velocity $[v] = 1.4 \times 10^5$ cm²/sec. The agreement between the calculated T_{1W} and the experimental T_1 for ^3He strongly supports the concept of ^3He bubbles in UT_3 . Although the closeness of the agreement may be fortuitous due to the uncertainties in t_s and T_{1S} , the calculation is probably accurate within an order of magnitude.

Recent measurements³⁶⁻³⁸ of the bubble sizes in helium implanted metals indicate an R_m of 25 Å is probably correct within a factor of 2 to 5. While a wide range of bubble sizes can be obtained in metal foils depending upon the irradiation conditions, low-energy (i.e., < 100 -keV) helium ions typically³⁶⁻³⁸ produce bubbles with nominal radii between 10–30 Å when the temperature during irradiation is below about 0.4 or 0.5 the metal melting point. Implantations at higher temperatures or post-irradiation anneals result in the formation of much larger bubbles, whose dimensions may approach³⁸ 1000 Å. Since the UT_3 samples were maintained at room temperature as ^3He was generated, the bubbles in UT_3 should closely resemble the helium size distribution in metals which were implanted at the lower temperatures. Although the distribution of helium bubbles in implanted metals are not likely to be identical with aged UT_3 , Blewer and

Maurin³⁹ found many similarities in the surface features of erbium metal and erbium deuteride films implanted with helium and aged erbium tritide films. However, the dimensions of the bubbles in heavily irradiated thin films typically^{6,37,39} vary between 1 and 50 μm , which is three to four orders of magnitude larger than the assumed bubble diameters in UT_3 . These large bubbles and blisters in the films are formed by the coalescence^{36,37} of many small bubbles (~ 30 – 50 Å diameters) at a critical concentration. Although similar coalescence processes may occur in bulk metal tritides, large (~ 1 – 50 - μm) bubbles have not been detected²⁸ in UT_3 powders and ^3He bubbles with $R_m \approx 25$ Å are reasonable approximations for the ^3He distribution.

If T_{2W} is approximately equal to T_{1W} , Eq. (20) yields $T_2 < T_{1W}$ and a T_2 in good agreement with the results in Table I and Fig. 9 when $\lambda \approx 6$ Å (i.e., approximately twice the molecular diameter of the ^3He atoms). However, both restricted diffusion in the magnetic field gradients and the semistatic dipolar interactions between ^3He nuclei near the bubble wall can affect T_2 . Hence, a quantitative calculation of T_2 is not possible, but a predicted T_2/T_{1W} ratio of ~ 0.2 for R_m of 25 Å is consistent with the experimental ^3He relaxation times. This qualitative agreement for T_{2m} provides a further justification of microscopic ^3He bubbles in the UT_3 samples.

Interactions with the conduction electrons and the uranium ions at the bubble wall, which dominate the ^3He relaxation times T_1 and T_{2m} , are responsible for the observed temperature and frequency behavior. Since the relaxation mechanisms at this paramagnetic surface are unknown, reliable evaluation is not possible. However, T_{1S}^{-1} is expected to be proportional to $(T - \theta)^{-1}$ below ~ 300 K as was found²⁰ for the proton spin-lattice relaxation time in UH_3 . This dependency produces a decrease in T_1 when the temperature is reduced and is seen in Fig. 9 for both T_1 and T_{2m} . Because T_2 for the ^3He spins is strongly influenced by T_{1W} , the observed T_{2m} reflects changes in T_{1S} , the major factor controlling T_{1W} . This idea is supported by the nearly constant T_{2m}/T_1 ratio between 200 and 300 K. The decrease in the ^3He relaxation times with frequency can be caused by either a stronger dipolar coupling through an increase in the magnetization with magnetic field strength or an inherent frequency dependence for T_{1S} . Although both explanations are plausible, insufficient information on the paramagnetic relaxation mechanisms in this system is available to examine their validity. Nevertheless, a frequency dependent T_{1W} is reasonable considering conduction electron overlap with a closed electronic shell atom. The frequency dependence for T_{2m} apparently levels off above 20

MHz, perhaps because the influence of the magnetization on mutual spin flipping has saturated.

In the limit of uniform dimensions for the ^3He bubbles, nearly exponential relaxation times are predicted¹⁰ when they are determined by surface interactions with the walls. However, nonexponential T_1 and T_{2m} are normally observed for ^3He in UT_3 as shown in Figs. 6 and 7. This behavior can occur if a distribution of bubble sizes exist in UT_3 . T_1 and T_{2m} are approximately proportional to R and R^2 , respectively, where R is the bubble radius. Each bubble has its own characteristic exponential relaxation times; however, the observed relaxation times for a macroscopic UT_3 sample are composed of the contributions for the entire distribution of ^3He bubble sizes. R_m in Eq. (24) now represents the mean bubble radius. Although the distribution of bubble sizes in UT_3 is unknown, it is expected to have the general form proposed by Gruber⁴⁰ for inert gas bubbles in reactor fuels. The majority of bubbles have radii near R_m with a rapid decrease in the number of bubbles below R_m but a much slower rate of decrease for bubbles larger than R_m . All ^3He bubbles contribute to the experimental relaxation time decays and yield nonexponential behavior as a general characteristic for these samples. Since an extremely large number of bubbles are involved and the bubble size distribution has not been determined for UT_3 samples, unique analyses of the magnetization decays cannot be obtained. Nevertheless, the general features of the experimental ^3He decays arise naturally as a direct consequence of a moderately sharply peaked distribution in bubble sizes. R_m is assumed to correspond to a magnetization decay of $1/e$ of the initial value. This approximation has been used in the present analyses of the ^3He relaxation times to describe the complex ^3He distribution in terms of the average parameter R_m .

In summary, detailed evaluations of the ^3He relaxation times in approximately 2–3-year-old UT_3 indicate that only microscopic gas bubbles can provide consistent agreement with the observed T_2^* , T_{2m} , and T_1 data. A range between about 20 and 100 Å is estimated for the mean radius of the ^3He gas bubbles. Because of insufficient knowledge of the nature of the relaxation mechanisms at the bubble wall and the bubble size distributions for UT_3 , quantitative comparisons between bubble properties and ^3He relaxation times cannot be performed. However, the basic correctness of the bubble properties has been established. The broad ^3He resonance signals (i.e., short T_2^* values) observed at the higher magnetic fields are produced by bulk susceptibility effects of the highly paramagnetic UT_3 material. Rigid-lattice interactions between immobile ^3He atoms in UT_3 sites have not been found.

IV. EFFECTS OF AGE ON HELIUM DISTRIBUTION

A. Experimental observations

The production rate of ^3He in UT_3 , which is controlled by the 12.3-year tritium half-life, increases the ^3He -to-T atom ratio by 1.55×10^{-4} /day. If all the ^3He generated in UT_3 is retained in the solid, the $^3\text{He}/\text{T}$ ratio would equal 0.167 after 1000 days. The actual ^3He retention in UT_3 obtained from volumetric analyses of gases released during decomposition at ~ 1300 K is presented in Fig. 10 where the $^3\text{He}/\text{T}$ ratios are normalized relative to the initial tritium content for each sample. The UT_3 retains approximately (95–100)% of the ^3He generated during the first several hundred days of aging. After about 700 days a dramatic increase in the helium release rate begins until only (55–60)% of the total ^3He produced is retained in 1600-day-old UT_3 . The results in Fig. 10 also indicate a nearly constant amount of helium ($^3\text{He}/\text{T}$ ratio of 0.12 ± 0.01) is retained in solid UT_3 after ~ 1200 days.

The ^3He relaxation times T_1 and T_{2m} for the five UT_3 preparations were measured during a 3-year period. Because of the differences in synthesis dates a total sample age of nearly 1700 days is represented by these relaxation times which are summarized in Fig. 11. Between 150 and 1200 days, T_1 and T_{2m} increase by factors of 2.5 and 15, respectively, and the T_{2m}/T_1 ratio increases from 0.04 and 0.23 during this time. The analysis in Sec. III for ^3He relaxation in gas bubbles indicate T_{1w} and T_{2w} are proportional to R_m and R_m^2 , respectively. Furthermore, the magnetic gradient contribution represented by Eqs. (10) and (11) decreases with R_m^2 . Hence, the behavior of the ^3He relaxation times observed between 150 and 1200 days in Fig. 11 and the strong evidence for microscopic ^3He gas bubbles in 2–3-year-old UT_3 imply a continual increase in average bubble size (i.e., mean radius R_m) as UT_3 ages. Although it is impossible to accurately establish the ^3He bubble dimensions from nuclear relaxation times alone, the observed changes in T_1 suggest R_m increases by a factor of ~ 3 during this period.

Other interpretations of the observed age dependence for T_1 and T_{2m} have serious difficulties. In the percolation model proposed⁸ for ^3He retention in TiT_x , ^3He atoms are trapped in interstitial sites and are immobile until a critical concentration, which permits the formation of interconnected pathways for rapid diffusion, is reached. This model requires the ^3He relaxation times to have a very small, nearly constant T_{2m}/T_1 ratio followed by an extremely large increase in this ratio at the critical concentration which occurs just before the onset of rapid ^3He -gas release. Since the ^3He relaxation times in Fig. 11 indicate the T_{2m}/T_1 ratio

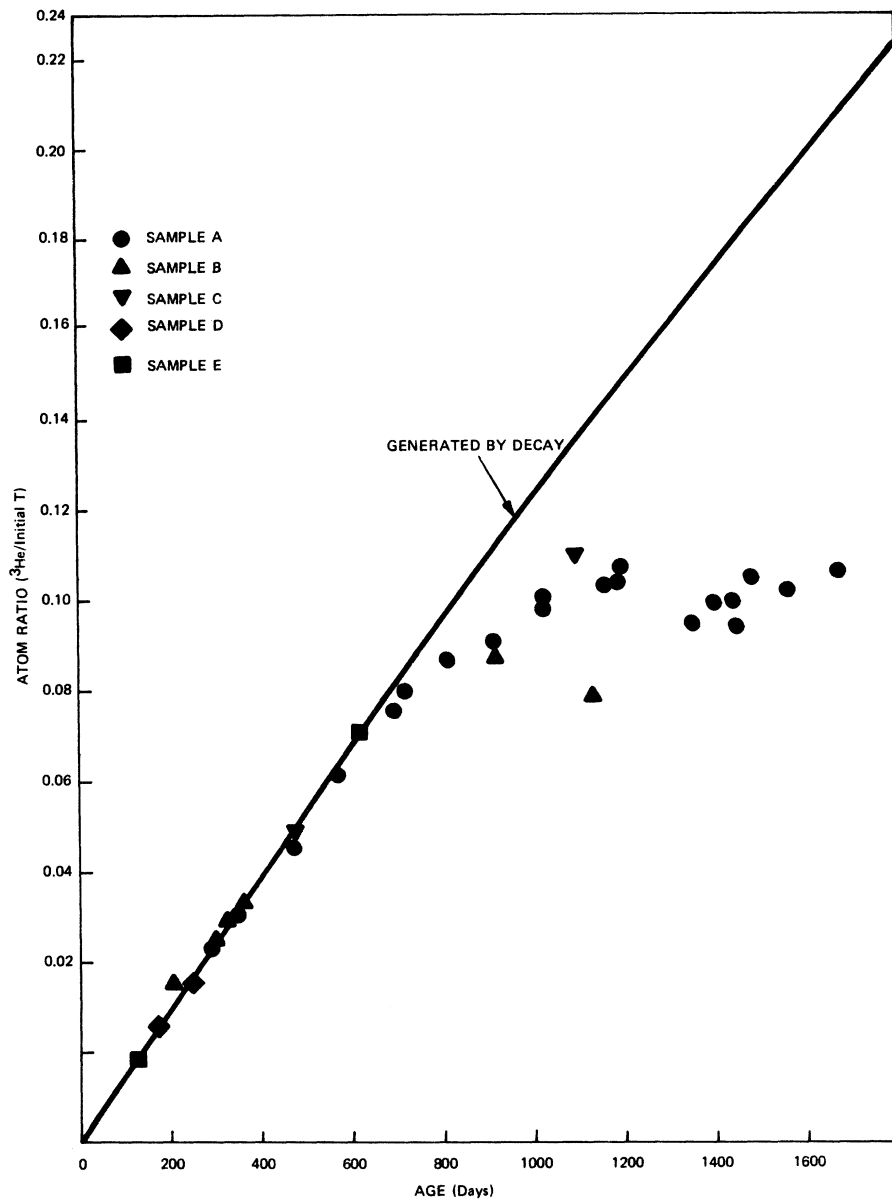


FIG. 10. Concentration of helium retained in UT_3 obtained during thermal decomposition of material from the five batches investigated by NMR. Solid curve is the ^3He produced by tritium decay.

for UT_3 increases smoothly for approximately 500 days past the start of rapid ^3He release, a percolation model cannot describe the observed age dependence. If the ^3He diffusivities become larger as UT_3 ages, a steadily rising T_{2m}/T_1 ratio as observed in Fig. 11 could occur. However, the increasing diffusion rates imply a high probability for measurable (i.e., $\geq 5\%$) ^3He release at low concentration and a gradual rather than the very abrupt change in the ^3He release rate. Neither of these features are found in Fig. 10.

After about 1200 days the ^3He relaxation times in Fig. 11 are observed to increase more slowly with age and apparently approach limiting values.

This behavior indicates the ^3He bubbles reach a maximum dimension as the ^3He concentration saturates during this period.

B. Discussion

A qualitative model for the retention of helium in UT_3 , which is consistent with the ^3He relaxation behavior determined during this study, can be developed from the formation, growth, and rupture of microscopic (i.e., $R_m < 500 \text{ \AA}$) gas bubbles. Since ^3He relaxation times in a 90-day-old UT_3 sample are indicative of mobile atoms in gas bubbles rather than interstitials, incipient bubbles are apparently formed before this time (i.e., a retained

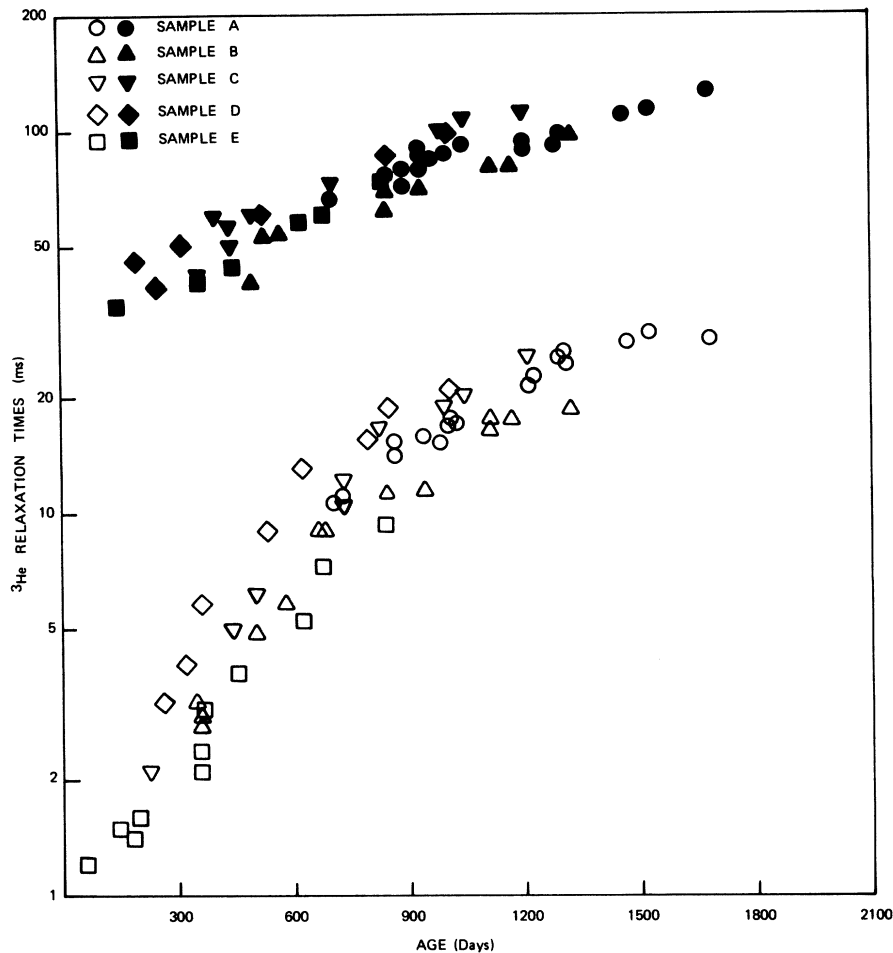


FIG. 11. Age dependence of ^3He relaxation times T_1 (closed symbols) and T_{2m} (open symbols). The measurements were performed at room temperature and 20 MHz with 400- μsec spacings between the π pulses in the CPMG sequence.

$^3\text{He}/\text{T}$ ratio below ~ 0.01). The helium atoms produced after the nucleation of these defects are assumed to be trapped in the bubbles or escape from a surface resulting in a vanishing small concentration of helium atoms in the UT_3 lattice. From an analysis of the dependence of initial helium release rates on the UT_3 surface areas, Wilson *et al.*⁴¹ deduced helium can directly escape the UT_3 lattice only from a surface layer about 50 Å thick, which corresponds to initial release rates of (1–2)% for the low surface area ($< 1 \text{ m}^2/\text{g}$) samples used in the present NMR studies. Wilson *et al.*⁴¹ also found the helium diffusion constant must be $10^{-18} \text{ cm}^2/\text{sec}$ or larger to obtain a steady state initial release rate within the first 50 days. Since the majority of helium atoms are formed in the crystal interior, most of the atoms are trapped in the bubbles which are expected to expand as their helium concentration increases. In accord with the nonexponential ^3He relaxation recoveries and the arguments of Gruber⁴⁰ a distribution of bubble sizes would exist. During the next several hun-

dred days the bubbles continue to grow without releasing significant quantities of helium gas. After about 700 days the largest bubbles exceed a critical dimension and irreversibly release their contents. Further aging results in more bubbles reaching the critical conditions and rupturing. Ultimately, release from the bubble rupturing processes can approximately equal the helium generation rate and would yield a nearly constant helium content in the UT_3 particles. During this period of rapid release the mean bubble radius R_m asymptotically approaches the critical dimension. The maximum R_m value is probably less than 100 Å from a consideration of the magnitude of T_1 values and the analysis in Sec. III. This rather simplistic model provides an acceptable explanation for the age dependence of helium retention and ^3He relaxation in UT_3 .

Other studies in progress at this laboratory and elsewhere indicate helium retention in UT_3 is a more complex phenomena than suggested by the above model. Although the present NMR measure-

ments provide convincing evidence for gas bubbles in UT_3 aged a few hundred days, both bubble nucleation and helium release processes are poorly understood. Rapid release probably occurs from grain boundaries as well as particle surfaces. The roles of vacancies in bubble formation and growth have not yet been established. The concept of a critical dimension for spontaneous bubble rupture cannot be verified with current data. If this parameter does represent the major helium release mechanism after about 700 days, it will be sensitive to numerous properties such as particle and grain size, dislocation distribution, stoichiometry, and impurity distribution. The actual rupturing of a bubble will depend on the mechanical strength and elasticity of the surrounding tritide lattice. Hence, a quantitative evaluation of helium retention in UT_3 is impossible without detailed characterization of the particle microstructures. Weaver in a very recent communication⁴² has arrived at a similar conclusion concerning the percolation model originally proposed⁸ for TiT_x . Although his further 3He relaxation-time measurements indicate the assumption of isolated 3He atoms is probably an oversimplification and evidence for growing 3He defects is given, NMR experiments are insufficient to completely explain helium retention. Nevertheless, NMR has yielded valuable microscopic insights on the distribution of helium in metal tritides.

V. CONCLUSIONS

The 3He distribution in UT_3 powders have been investigated by pulse NMR techniques. Detailed analyses of the frequency, temperature, and age dependence of the 3He resonance linewidths and relaxation times indicate microscopic gas bubbles are formed in the UT_3 particles. The radii of these bubbles are estimated to be $\leq 100 \text{ \AA}$. Because UT_3 is a highly paramagnetic material, inhomogeneous

magnetic gradients influence the 3He linewidths and relaxation times. All of the major features of the NMR parameters can be described by spin relaxation at bubble walls and magnetic gradient effects. The occupancy of UT_3 lattice sites by more than $10^{20} \text{ } ^3He$ atoms/g was found to be unlikely.

A qualitative model for the observed helium retention in UT_3 has been obtained from the NMR measurements. In this model, 3He bubbles are nucleated at a relatively young age and grow primarily by trapping the 3He atoms essentially upon generation by tritium decay. Although the diffusion coefficient for 3He atoms in the UT_3 lattice cannot be established from the present studies, the analysis of Wilson *et al.*⁴¹ indicates a lower limit of about $10^{-18} \text{ cm}^2/\text{sec}$ should be sufficient to permit rapid trapping of the 3He atoms in uniformly distributed microscopic gas bubbles. The predominant release mechanism is bubble rupture at a critical dimension. Although this model yields a reasonable description for 3He behavior in UT_3 , additional investigations (probably, involving multiple techniques) are required for a quantitative evaluation of the mechanisms involved.

ACKNOWLEDGMENTS

The authors wish to express their appreciation to J. Glaub and G. Mullins for preparing the NMR samples, R. Sprague for performing the thermal decompositions, R. Eckstein for the x-ray diffraction measurements, and Dr. H. Weaver for performing the cw measurements of the tritium resonance in two UT_3 samples. Beneficial discussions were held with Dr. W. Bauer, Professor R. Cotts, G. Downs, Dr. M. Malinowski, Dr. M. Schwab, Dr. H. Weaver, Dr. C. Wiedenheft, and Dr. K. Wilson. The continual support of Dr. R. DeSando is also appreciated.

*Operated for the U. S. ERDA under Contract No. EY-76-C-04-0053.

¹A. M. Rodin and V. V. Surenyants, *Fiz. Metal. Metalloved* **10**, 216 (1960).

²P. M. S. Jones, Atomic Weapons Research Establishment (UKAEA) Report No. 0-27/67 (1967) (unpublished).

³P. M. S. Jones, W. Edmonson, and W. J. McKenna, *J. Nucl. Mater.* **23**, 309 (1967).

⁴V. P. Vertebnyi, M. F. Vlaser, A. L. Kirilyuk, R. A. Zatserkovskii, M. V. Pasechnik, and V. A. Stepanenko, *At. Energy (USSR)* **22**, 235 (1967).

⁵A. M. Rodin and V. V. Surenyants, *Russ. J. Phys. Chem.* **45**, 612 (1971).

⁶L. C. Beavis and C. J. Miglionico, *J. Less-Common Metals* **27**, 201 (1972).

⁷P. C. Souers, T. A. Jolly, and C. F. Cline, *J. Phys. Chem. Solids* **23**, 1717 (1967).

⁸H. T. Weaver and W. J. Camp, *Phys. Rev. B* **12**, 3054 (1975).

⁹J. H. Van Vleck, *Phys. Rev.* **74**, 1168 (1948).

¹⁰R. C. Wayne and R. M. Cotts, *Phys. Rev.* **151**, 264 (1966); R. Robertson, *ibid.* **151**, 273 (1966).

¹¹H. Meyer, *J. Appl. Phys.* **39**, 390 (1968).

¹²D. Zamir and R. M. Cotts, in *Proceedings of Thirteenth Ampere Colloque*, edited by L. Van Gervan, Ed. (North-Holland, Amsterdam, 1965), p. 276.

¹³Scanning electron microscopy (Mound Laboratory) studies by G. Downs indicate the UT_3 particles are extremely irregular with a wide distribution of particle sizes between $\sim(0.1-20) \mu\text{m}$. The larger particles are composed of columnar substructures with diameters $\sim 0.1-0.5 \mu\text{m}$.

¹⁴Q. Johnson, T. J. Viel, and H. R. Leider, *J. Nucl. Mater.* **60**, 231 (1976).

- ¹⁵S. Meiboom and D. Gill, *Rev. Sci. Instrum.* **29**, 1688 (1958).
- ¹⁶J. Grunzweig-Genossar, M. Kuznietz, and B. Meero-vici, *Phys. Rev. B* **1**, 1958 (1970).
- ¹⁷L. E. Drain, *Proc. Phys. Soc. Lond.* **80**, 1380 (1962).
- ¹⁸N. Boden and M. Gibb, *Mol. Phys.* **27**, 1359 (1974).
- ¹⁹R. C. Bowman, Jr. and A. Attalla, in *Radiation Effects and Tritium Technology for Fusion Reactors*, edited by J. S. Watson and F. W. Wiffen, CONF-750989, Vol. IV, 1976 (unpublished), p. IV-68.
- ²⁰G. Cinader, M. Peretz, D. Zamir, and Z. Hadari, *Phys. Rev. B* **8**, 4063 (1973).
- ²¹M. Peretz, D. Zamir, G. Cinader, and Z. Hadari, *J. Phys. Chem. Solids* **37**, 105 (1976).
- ²²H. T. Weaver (private communication).
- ²³A. Abragam, *Principles of Nuclear Magnetism* (Oxford, London, 1962).
- ²⁴R. M. Cotts, *Ber. Bunsenges. Phys. Chem.* **76**, 760 (1972).
- ²⁵H. T. Weaver and W. Beezhold, *J. Nucl. Mater.* **53**, 346 (1974).
- ²⁶H. T. Weaver and W. Beezhold, *Appl. Phys. Lett.* **24**, 522 (1974).
- ²⁷R. Chapman and M. G. Richards, *Phys. Rev. Lett.* **33**, 18 (1974).
- ²⁸G. Downs (private communication).
- ²⁹R. S. Barnes, *J. Nucl. Mater.* **11**, 135 (1964).
- ³⁰J. H. Evans, *J. Nucl. Mater.* **61**, 1 (1976).
- ³¹B. T. Beal and J. Hatton, *Phys. Rev.* **139**, 1751 (1965).
- ³²J. S. Karra and G. E. Kemmerer, Jr., *Phys. Lett. A* **33**, 105 (1970).
- ³³W. A. Fitzsimmins, L. L. Tankersley, and G. K. Walters, *Phys. Rev.* **179**, 156 (1969).
- ³⁴R. S. Timset, J. M. Daniels, and A. D. May, *Can. J. Phys.* **49**, 560 (1971).
- ³⁵R. Chapman and M. Bloom, *Can. J. Phys.* **54**, 861 (1976).
- ³⁶J. H. Evans, *Nature* **256**, 299 (1975).
- ³⁷J. H. Evans, *J. Nucl. Mater.* **61**, 117 (1976).
- ³⁸E. Ruedl, O. Gautsch, and E. Staroste, *J. Nucl. Mater.* **62**, 63 (1976); D. J. Mazey, B. L. Eyre, J. H. Evans, S. K. Erents, and G. M. McCracken, *ibid.* **64**, 145 (1977).
- ³⁹R. S. Blewer and J. K. Maurin, *J. Nucl. Mater.* **44**, 260 (1972).
- ⁴⁰E. E. Gruber, *J. Appl. Phys.* **38**, 243 (1976).
- ⁴¹K. L. Wilson, M. E. Malinowski, and M. I. Baskes, Sandia Laboratories Report SAND No. 76-8221, 1976 (unpublished).
- ⁴²H. T. Weaver, *Appl. Phys. Lett.* **30**, 80 (1977).